biomass

MDPI

Article

Hydrochar from Spent Coffee Ground as a Sustainable Adsorbent for Dye Removal from Water: Adsorption Characterization and Improvement via Soft Alkaline Activation

Gennaro Pace [1], Gianluigi Farru [2], Fabiano Asunis [2], Giovanna Cappai [2], Angela De Bonis [3], Maria Cristina Mascolo [4,5,6], Donatella Caniani [1], Ignazio Marcello Mancini [1], Salvatore Masi [1] and Francesco Di Capua [1,*]

1 Department of Engineering, University of Basilicata, Via Dell'Ateneo Lucano 10, 85100 Potenza, Italy
2 Department of Civil and Environmental Engineering and Architecture, University of Cagliari, Via Marengo 2, 09123 Cagliari, Italy
3 Department of Sciences, University of Basilicata, Via Dell'Ateneo Lucano 10, 85100 Potenza, Italy
4 Department of Letter and Philosophy, University of Cassino and Southern Lazio, Via S. Angelo—Località Folcara, 03043 Cassino, FR, Italy
5 Materials Laboratory—Department of Civil and Mechanical Engineering, University of Cassino and Southern Lazio, Via Gaetano di Biasio 43, 03043 Cassino, Italy
6 Institute of Environmental Geology and Geoengineering, National Research Council, Area della Ricerca di Roma 1, Via Salaria Km 29.300, C.P. 10, Monterotondo Stazione, 00015 Rome, Italy
* Correspondence: francesco.dicapua@unibas.it

Abstract

Spent coffee grounds (SCGs) are abundantly produced worldwide as a by-product of coffee brewing, and production is surging following the rise in global coffee consumption. Although the adsorption properties of raw SCGs have been investigated in previous studies, limited attention has been paid to the use of SCG-derived hydrochars as engineered adsorbents. In this work, hydrochars produced via hydrothermal carbonization (HTC) of SCGs at different temperatures were systematically assessed for their capacity to remove methylene blue (MB) dye from aqueous solution. The effect of HTC temperature and soft alkaline activation on MB adsorption were evaluated through adsorption batch tests. The soft alkaline activation increased the experimental adsorption capacity from <20 mg g^{-1} for untreated hydrochars to approximately 100 mg g^{-1} at 20 °C, while Langmuir isotherm analysis yielded a monolayer capacity of 147.1 mg g^{-1} at the same temperature; experimental uptake further increased to 215.6 mg g^{-1} at 40 °C and high dye concentrations. Kinetic, isotherm, and thermodynamic tests were performed on selected materials to describe their adsorption behavior and potential mechanisms. Microscopic, diffraction, spectroscopic, and porosimetric analyses were performed to investigate the structural differences among the tested materials. This study shows that temperature regulation and soft alkaline activation can strongly improve the adsorption capacity of the hydrochars, producing competitive low-cost adsorbents from a waste material in compliance with the principles of the circular economy.

Keywords: adsorption; hydrochar; spent coffee ground; soft alkaline activation; methylene blue; wastewater

Academic Editor: Ulla Lassi

Received: 26 November 2025
Revised: 23 December 2025
Accepted: 30 December 2025
Published: 7 January 2026

1. Introduction

The coffee industry produces a substantial amount of waste globally, with spent coffee grounds (SCGs) being one of the most prevalent by-products. SCGs are the remnants

of coffee after brewing, and their disposal presents both environmental and economic challenges. It is estimated that approximately 6 million tons of SCGs are generated annually worldwide [1]. This large quantity of waste is primarily discarded in landfills, contributing to waste accumulation and environmental degradation. The global coffee industry is valued at over USD 100 billion, with an average consumption of 500 billion cups per year, and the demand for coffee continues to rise due to its global popularity [2]. As the coffee market grows, the generation of SCGs will only increase, amplifying the need for sustainable waste management solutions.

However, this waste stream is not without value. Recent studies have demonstrated that SCGs contain a variety of bioactive compounds, including antioxidants, polyphenols, lipids, and carbohydrates, which make them a promising resource for various industrial applications [3]. Therefore, SCGs have gained significant attention due to their potential as a sustainable resource in the production of biofuels, biopolymers, and as an ingredient in food and cosmetics [4]. Moreover, their rich organic composition suggests that they could be used for soil enhancement, providing valuable nutrients for agriculture [5]. Despite the growing interest in recycling and repurposing SCGs, challenges remain in terms of developing efficient processes for large-scale utilization while minimizing environmental impacts [6].

A particularly promising application of SCGs lies in wastewater treatment, specifically in the adsorption of contaminants such as dyes and pigments, which are commonly found in industrial effluents, e.g., from the textile industry. Due to their porous structure and the presence of functional groups on their surface, SCGs have been studied extensively for their ability to adsorb various dyes from aqueous solutions [7]. Several studies have demonstrated that SCGs exhibit strong adsorptive properties for a wide range of organic dyes, including methylene blue (MB), malachite green, rhodamine B, and Congo red, making them a cost-effective and environmentally friendly alternative to traditional adsorbents such as activated carbon [8–11].

In addition to these applications, another innovative approach to processing organic waste, including SCGs, is hydrothermal carbonization (HTC), a thermochemical process that converts wet organic materials into a solid, carbon-rich product known as hydrochar. HTC takes place at temperatures typically between 180 and 250 °C and pressures of 2–6 MPa for 5 to 240 min in the presence of water [12]. This process not only reduces the volume of the organic waste in view of its disposal, but also enhances its density and stability, making the hydrochar a valuable material for various applications, including energy production, soil amendment, and environmental remediation [13].

In particular, hydrochar derived from SCGs has shown promising performance in the removal of heavy metals, organic dyes, and pharmaceuticals from wastewater [14]. Nevertheless, hydrochars typically feature low surface areas, placing a pivotal role on the surface functionalities to provide adsorption sites for the contaminants. HTC was observed to impact the presence of functional groups on the material surface, e.g., by the loss of oxygen-containing functional groups, depending on the HTC temperature and residence time [15]. Therefore, chemical/physical activation is generally needed to modify the surface functionality and enhance the adsorption capacity of the produced hydrochar [12,15]. Chemical activation involves treating the hydrochar with activating agents such as potassium hydroxide or phosphoric acid, which not only increase the surface area but also introduce additional functional groups on the surface, further enhancing the material's ability to capture pollutants [15]. On the other hand, physical activation typically involves exposing the hydrochar to high temperatures (800–1100 °C) in the presence of gases such as steam or carbon dioxide, which increases its surface area and pore volume, thus improving its capacity to adsorb contaminants [12,15]. The combination of both activation

methods could synergistically enhance the adsorption capacity of the produced hydrochar. Moreover, performing activation at lower temperatures would enhance the economic and environmental sustainability of adsorbent production from hydrochar. Recently, Cuccarese et al. [10] proposed soft alkaline activation, a method consisting in impregnating the SCGs with sodium hydroxide (NaOH) and carbonizing the resulting material at 300 °C as a more cost-effective method to enhance the adsorption properties of SCGs. Similarly, such a method may be applied to enhance the adsorption potential of SCG-derived hydrochars, producing a valuable and low-cost adsorbent from waste residues.

This study investigates the adsorption capacity of hydrochars produced from HTC of SCGs at different temperatures. Raw feedstock and HTC products are compared in terms of physical/chemical characteristics and adsorption potential for the removal of MB from water. The effect of soft alkaline activation on improving the adsorption capacity of the SCG-derived hydrochar is also investigated. To the best of our knowledge, dye adsorption on SCG hydrochars was not systematically investigated in previous studies; in this study, MB is employed as a model dye to elucidate adsorption of raw and mildly activated SCG hydrochars. The kinetics, isotherms, and thermodynamics of the process, as well as the effects of initial MB concentration and temperature, are elucidated. Overall, the study aims to contribute to circular economy practices by converting HTC residues into valuable materials for environmental remediation.

2. Materials and Methods

2.1. Materials Preparation and Characterization

SCGs were collected from a coffee shop near the Engineering Faculty of the University of Cagliari (Italy). The collected SCGs were stored in sealed plastic containers at 4 °C until further processing.

HTC experiments were conducted using a Berghof BR-1000 high-pressure reactor with a total volume capacity of 1.5 L. The reactor is designed to operate under high temperatures and pressures, featuring a PTFE lining for chemical resistance. The reactor was loaded with SCG and distilled water to achieve a 10% solid content. The system was sealed and heated to the desired temperature. The SCG was processed at 220 °C (SCG_220) and at 240 °C (SCG_240) for 1 h. The heating rate was controlled to reach the target temperature within approximately 1 h and the selected temperature (±1 °C) was maintained for the specified duration. After the reaction, the reactor was allowed to cool naturally to room temperature before opening.

Upon completion of the HTC process, the solid fraction (hydrochar) and the liquid fraction (process water) were separated using a filter press. The hydrochar was then dried in a laboratory oven at 105 °C overnight to remove residual moisture. Dried samples were stored in sealed plastic bags for subsequent analyses. Each sample was labeled according to the feedstock and operational conditions.

Hydrochar activation was performed via alkaline washing followed by low-temperature carbonization. Initially, 5 g of SCG-derived hydrochar was stirred in 200 mL of 1 M NaOH solution for 6 h. Subsequently, the material was carbonized in a ceramic crucible at 300 °C in an oven overnight. In this step, water completely evaporated and no liquid effluent was generated. Such an activation method is also referred to as soft alkaline activation [10]. After cooling to room temperature, the material was crushed with a pestle. The materials were not washed to avoid generation of a liquid residue during synthesis. The activated hydrochars were labeled as SCG_220_a and SCG_240_a.

Before adsorption tests, all materials were ground with an electric coffee grinder to homogenize their particle size as much as possible and to determine the potential influence of particle-size effects on adsorption kinetics and equilibrium behavior. The

structure and physical–chemical properties of the adsorbent materials were characterized by X-ray Diffraction (XRD), Raman spectroscopy, Fourier-transform infrared spectroscopy (FTIR), Scanning Electron Microscopy (SEM), energy-dispersive X-ray (EDX) spectroscopy, Brunauer-Emmett-Teller (BET) analysis, and Mercury Intrusion Porosimetry (MIP).

2.2. Adsorption Tests

Adsorption tests were performed to compare the adsorption capacity of raw SCGs and derived hydrochars (untreated and activated) as well as the adsorption kinetics, isotherms, and thermodynamics of the hydrochars for the removal of MB from water. The tests were performed in batch mode in 50 mL plastic vials placed on a rotary shaker (Argolab, Carpi, Italy) at the speed of 200 rpm for 180 min to ensure adequate mixing and time to reach the equilibrium. All tests were performed in triplicate. The experimental data are visually represented as average ± standard deviation (error bars). 200 mg of adsorbent material were added to each vial before adding the MB solution, resulting in an adsorbent concentration of 4 g L^{-1}. All materials were ground in a coffee grinder before the tests to obtain a uniform particle size. MB trihydrate ($C_{16}H_{18}N_3SCl{\cdot}3H_2O$, Reag. Ph. Eur.) was purchased from Carlo Erba (Cornaredo, Italy) and mixed with distilled water to prepare solutions at different concentrations. The pH of the MB solutions without pH adjustment was in the range of 6.5–7. The list of tests and experimental conditions is reported in Table 1.

Table 1. A list of the experiments performed to assess the adsorption characteristics of SCG materials.

Test	Materials	MB Concentration (mg L^{-1})	Temperature (°C)
1—Comparative tests (HTC effect)	SCG SCG_220 SCG_240	250	20
2—Comparative test (activation effect)	SCG_220_a SCG_240_a	250	20
3—Comparative test (pH effect)	SCG	250 (pH 11)	20
4—Kinetics	SCG SCG_240 SCG_240_a	250	20
5—Isotherms and effect of initial MB concentration	SCG_240_a	100, 250, 500, 750, 1000	20
6—Thermodynamics and effect of temperature	SCG_240_a	100, 250, 500, 750, 1000	5, 20, 40

2.2.1. Comparative Tests

Batch adsorption tests were performed to compare the adsorption capacity of the raw SCGs, SCG hydrochars produced at 220 and 240 °C, and activated hydrochars to assess the effect of HTC and soft alkaline activation on the adsorption properties of SCGs. Additionally, the effect of alkaline pH on MB adsorption with raw SCGs was tested to have a more meaningful comparison with the activated SCG hydrochars. The pH was adjusted to 11 by using a 1 M NaOH solution. The comparative adsorption tests were performed with a MB concentration of 250 mg L^{-1} at 20 ± 2 °C (Table 1). Liquid samples were withdrawn from the vials at different time intervals to measure MB concentration and calculate the adsorption capacity at different time intervals. The adsorption capacity q was evaluated according to Equation (1):

$$q = \frac{mass\ of\ MB\ adsorbed\ (mg)}{mass\ of\ adsorbent\ (g)} = \left(c_i - c_f\right) \cdot \frac{V}{m} \quad (1)$$

2.2.2. Kinetic and Isotherm Tests

Kinetic and isotherm tests were run to investigate the adsorption mechanisms of selected SCG materials (see Table 1). Isotherm tests also allowed to estimate the influence of the initial MB concentration on the q_e value.

Adsorption kinetics were evaluated in batch tests at an initial MB concentration of 250 mg L^{-1} and a temperature of 20 (±2) °C. The test vials were sampled at 5, 20, 40, 60, 120, and 180 min. Five kinetic models, i.e., pseudo-first order, pseudo-second-order, intraparticle diffusion, Elovich, and liquid film diffusion, were considered.

Adsorption isotherms were evaluated by performing batch tests at different initial MB concentrations, i.e., 100, 250, 500, and 750 mg L^{-1}, and 20 (±2) °C. Liquid samples were collected at the beginning and at the end (180 min) of the test. The isotherm models that were considered for the best fitting of the experimental data were Langmuir, Freundlich, Temkin, and Dubinin–Radushkevich. Additionally, the Langmuir isotherm dimensionless constant R_L, also known as the equilibrium parameter, was calculated as reported by McKay [16]:

$$R_L = \frac{1}{1 + K_L \cdot C_0} \quad (2)$$

The value of R_L indicates whether the adsorption process is favorable ($0 < R_L < 1$), unfavorable ($R_L > 1$), irreversible ($R_L = 0$), or linear ($R_L = 1$).

Table 2 lists the kinetic and isotherm models considered in this study and their linear equations. For both kinetic and isotherm tests, the fitting of the experimental data to each model was evaluated by linear regression analysis with the least squares method.

Table 2. Kinetic and isotherm models considered to describe MB adsorption with SCG materials.

Test	Model	Linear Equation
Kinetic	Pseudo-first order	$log(q_e - q_t) = log\,(q_e) - k_1 t$
	Pseudo-second order	$\frac{t}{q_t} = \frac{1}{k_2 q_e^2} + \frac{t}{q_e}$
	Intraparticle diffusion	$q_t = k_{dif} t^{1/2} + C$
	Liquid film diffusion	$ln\left(1 - \frac{q_t}{q_e}\right) = -k_{fd} t$
	Elovich	$q_t = \frac{1}{\beta} ln(\alpha\beta) + \frac{1}{\beta} ln(t)$
Isotherm	Langmuir	$\frac{C_e}{q_e} = \frac{1}{K_L q_m} + C_e/q_m$
	Freundlich	$\ln q_e = \ln K_f + \frac{1}{n_F} ln C_e$
	Temkin	$\frac{q_e}{q_m} = \frac{RT}{b_T} \ln A C_e$
	Dubinin–Radushkevich	$\ln q_e = \ln q_s - \beta\varepsilon^2$ $\varepsilon = RTln(1 + \frac{1}{C_e})$ $E = \frac{1}{-\sqrt{2\beta}}$

2.2.3. Thermodynamic Analysis

The thermodynamics of the adsorption process were evaluated through batch adsorption tests performed at different temperatures. The tests allowed the investigation of the effect of temperature on MB adsorption by activated hydrochars, as well as the evaluation of the Gibbs free energy, enthalpy, and entropy of the adsorption process. Three different temperatures were selected for the tests, i.e., 5, 20 and 40 °C. The minimum and maximum temperatures were maintained by placing the rotary shaker in an incubator (ISCO, Lincoln, NE, USA), while the test at medium temperature was carried out in a temperature-controlled room maintained at 20 (±2) °C. The MB solution was placed in the incubator at the selected temperature 24 h before the test.

The following equations were adopted to evaluate the thermodynamic parameters for the adsorption process:

$$\Delta G^\circ = -RT \ln K_a \quad (3)$$

$$\Delta G^\circ = \Delta H^\circ - \mathrm{T}\,\Delta S^\circ \quad (4)$$

According to Liu [17], K_a can be reasonably approximated by the distribution constant $K_c = \mathrm{C_{ad}}/\mathrm{C_e}$. By combining Equations (3) and (4) the following equation is obtained (Equation (5)):

$$\ln K_a = -\frac{\Delta H^\circ}{RT} + \frac{\Delta S^\circ}{R} \quad (5)$$

By plotting $\ln K_a$ versus $1/\mathrm{T}$, it is possible to estimate the enthalpy and entropy of the adsorption process.

2.3. Statistical Analysis

The fitting of the isotherm and kinetic models with experimental data was evaluated according to the coefficient of linear determination and other error functions including the sum of the squares of the errors (SSE), the residual root mean square error (RMSE) and the chi-square test (χ^2) (Equations (6)–(9)).

$$R^2 = \frac{1 - \sum_{n=1}^{n}(q_{e,n} - q_{m,n})^2}{\sum_{n=1}^{n}(Q_{e,n} - Q_{m,n})^2} \quad (6)$$

$$SSE = \sum_{n=1}^{n}(q_{e,n} - q_{m,n})^2 \quad (7)$$

$$RMSE = \sqrt{\frac{1}{n-1}\sum_{n=1}^{n}(q_{e,n} - q_{m,n})^2} \quad (8)$$

$$\chi^2 = \sum_{n=1}^{n}\frac{(q_{e,n} - q_{m,n})^2}{q_{e,n}} \quad (9)$$

The statistical difference in the adsorption capacity profiles obtained with the different SCG materials was assessed by one-way analysis of variance (ANOVA) using Excel 365 (Microsoft, Redmond, WA, USA).

2.4. Analytical Methods

Chemical analyses. The concentration of MB in the liquid samples was measured spectrophotometrically with a 7600 UV-Vis spectrophotometer (WTW, Wuppertal, Germany). The absorbance spectrum of the MB solutions showed the maximum absorbance at a wavelength of 665 nm, which was selected for the analysis. The pH of the liquid samples was measured with a PC 7 Vio multiparameter equipped with a Sensor Elettrodo 201T DHS probe (XS, Carpi, Italy).

Solid-phase analyses. Spectroscopic characterization of all samples was conducted by the FTIR and microRaman techniques. FTIR spectra were acquired by using a JASCO 4000 (JASCO, Tokyo, Japan) instrument operating in the 400–4000 $\mathrm{cm^{-1}}$ spectral range and with a resolution of 4 $\mathrm{cm^{-1}}$. Raman spectra were acquired by using a Jobin-Yvon Horiba LabRam spectrometer (HORIBA, Kyoto, Japan), equipped with an Olympus microscope with 10×, 50× and 100× objectives. The excitation source was He-Ne laser (λ = 632.8 nm). Spectra were acquired with a 600 g/mm holographic grating, obtaining a resolution of 4 $\mathrm{cm^{-1}}$. A SIEMENS D5000 diffractometer (Siemens, Munich, Germany) was used to acquire XRD spectra. The instrument was operated at 40 kV and 32 mA, using CuKα radiation, in a q-2q configuration. The spectra have been acquired at 2θ = 5–60°, stepsize 0.040°, time per step 4 s. The surface images were taken by SEM, using a Philips microscopy (XL series, Almelo, The Nederland) and the chemical composition were analyzed using EDX with a

DX.4 detector (EDAX, Mahwah, NJ, USA). Brunauer–Emmett–Teller (BET) surface area and micro-mesoporosity (BJH method) were measured, after products were vacuum-dried at 80 °C for 4 days, by adsorption/desorption isotherms of N_2 performed at 77 K according to the BET method, using a Gemini instrument from Micromeritics (Norcross, GA, USA). The linear range used for BET measurement was between 0.1 and 0.3 for relative pressures P/P0. In this range, the correlation constant R^2 is 0.999–1.000. The extent of the uncertainties is reported in Table S1. Meso-macro porosity was measured by MIP with an Autopore III (Micromeritics, Norcross, GA, USA).

3. Results and Discussion

3.1. Physical–Chemical Properties of the SCG Adsorbent Materials

The FTIR, Raman, and XRD characterization of the SCG materials utilized in this study as adsorbents for MB removal is shown in Figure 1.

The FTIR spectra of untreated and activated hydrochars and of raw SCGs are displayed in Figure 1A. Compared with the spectrum of the raw SCG, some difference in the chemical structure of the carbonaceous material can be spotted after the HTC treatment. The bands centered at 3250 and 2850 and 2910 cm^{-1}, related to the stretching of the O-H and C-H groups, respectively, decrease with increasing the operational temperature of the HTC process. At the same time, the signal of the stretching vibration of the carbonyl (C=O) group at 1700 cm^{-1} appears after the hydrothermal treatment, whereas the signal at 1740 cm^{-1}, related to C=C stretching disappears.

The soft alkaline activation process also imparted specific modifications to the SCG-derived hydrochars. In particular, two specific bands appear at 1410 and 1640 cm^{-1}. The peak at 1410 cm^{-1} is due to the stretching vibration of carbonate (CO_3^{2-}), whereas the peak at 1640 cm^{-1} can be related to the bending vibration of H_2O molecules. Moreover, the signal of O-H stretching mode becomes very intense. These characteristics comply well with the soft alkaline activation process, which consisted in an alkaline washing of the hydrochars with a strong NaOH solution followed by carbonization at 300 °C. Based on the FTIR spectra of the activated hydrochar, this process led to the precipitation of carbonate, presumably sodium carbonate ($NaCO_3$), while the material surface could be refunctionalized by the hydroxyl groups of NaOH, which were partially lost during the HTC process.

The Raman spectrum (Figure 1B) of the raw SCG adsorbent is dominated by a large structureless luminescence band related to the presence of conjugated and hydrogenated functionalities, as suggested by the FTIR spectrum. Increasing the temperature of the HTC process led to the formation of an amorphous carbon-like material, as suggested by the presence of the D (defect band) and G (graphitic band) bands centered at about 1340 and 1565 cm^{-1}, respectively. The G and D bands were de-convoluted using a Lorentzian line shape, in order to obtain the I_D/I_G ratio, which is proportional to the sp^2/sp^3 ratio and is one of the relevant parameter to evaluate the structure of amorphous carbon materials. An increase in the I_D/I_G ratio after the hydrochars activation was observed, irrespective of the initial HTC temperature, suggesting a higher degree of structural disorder [18]. In the spectra of the hydrochars, a signal at 1066 cm^{-1}, related to CO_3^{2-}, is clearly distinguishable.

The presence of $NaCO_3$ in the activated hydrochars is confirmed by the XRD analysis (Figure 1C). The diffractograms of the hydrochars obtained at 220 and 240 °C are dominated by a broad band centered at 2θ = 20°, confirming the amorphous character of the prepared materials, whereas the narrow peak at 2θ = 21.4° suggests the presence of residual functionalities. After activation, new narrow peaks appeared. All reflections in the SCG_240_a material are related to monoclinic sodium bicarbonate, $Na_3H(CO_3)_2{\cdot}2H_2O$ (JCPDS n. 00-029-1447), and sodium carbonate (JCPDS n. 00-018-1208). The presence of

sodium carbonate and bicarbonate, confirmed by FTIR and XRD analyses, likely influenced the adsorption behavior of the activated hydrochars. Carbonate species increase the surface basicity and promote electrostatic attraction between the negatively charged surface and the cationic MB molecules, especially at alkaline pH [19]. However, their partial occupation of surface mass may also reduce the carbon fraction available for π–π interactions. The overall enhancement in adsorption capacity (as described in the following sections) suggests that the positive effects on surface charge and hydrophilicity outweigh the potential blocking of carbonaceous sites.

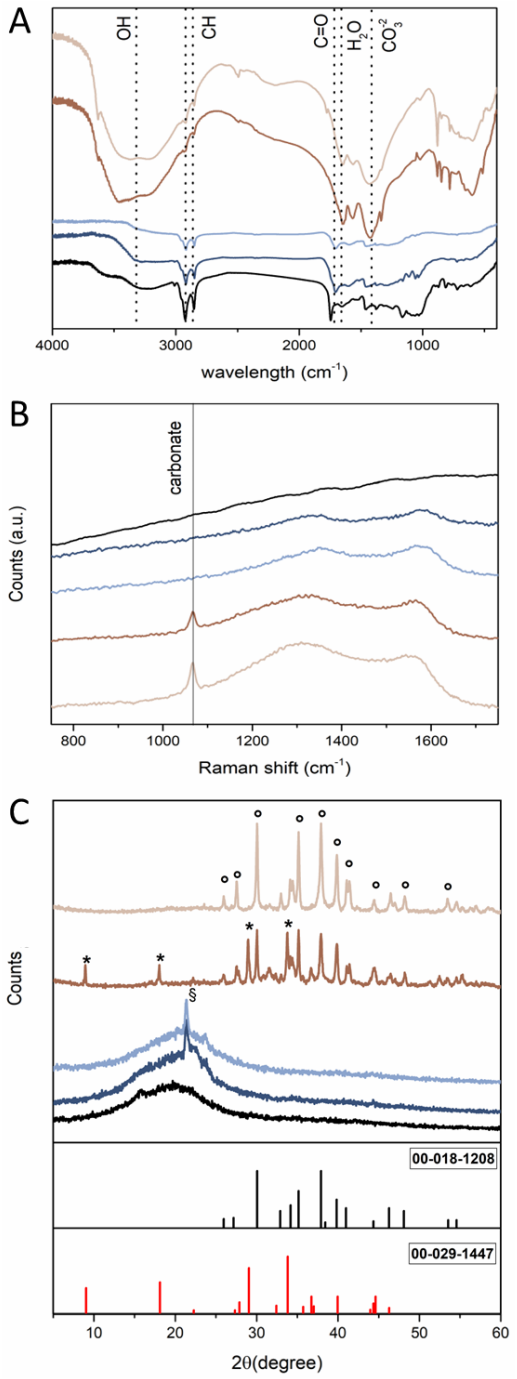

Figure 1. FTIR (**A**), Raman (**B**), and XRD (**C**) spectra of raw SCGs (black line) and SCG hydrochars produced at 220 °C and 240 °C before (dark and light blue lines, respectively) and after (dark and light brown lines, respectively) activation. In XRD diffractograms, * = sodium hydrogen carbonate hydrate [00-029-1447], ° = sodium carbonate [00-018-1208], § = stearic acid [00-004-0364]).

Figure 2 shows the SEM micrographs of SCG materials listed in Table 1. Raw SCG (Figure 2a) presents a relatively uniform grain size distribution with the majority of grains ranging from 200 to 300 microns (Figure 2f). In contrast the other materials (Figure 2b–e), consist predominantly of smaller (Figure 2n–q) and coarser particles (Figure 2g,h,i,l), with a more heterogeneous morphology. Notably, raw SCG displays an alveolar porous structure (Figure 2f) with macropores of micrometric size (Figure 2l,m). SEM images clearly show that hydrothermal treatment caused a collapse of this original microstructure. In fact, both activated and non-activated hydrochars present more compact and irregularly shaped grains (Figure 2h,i,l) made up of aggregates of particles of varying size (in the micrometer range), indicating a significant morphological transformation due to the treatment.

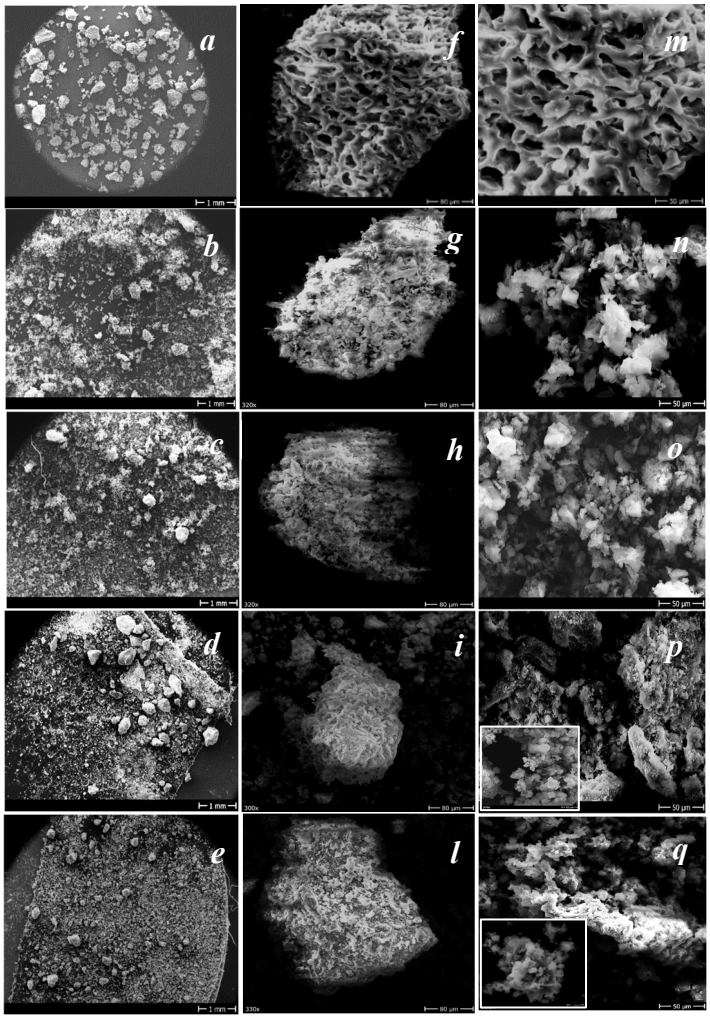

Figure 2. SEM micrographs of sample SCG0 (**a**,**f**,**m**), SCG_220 (**b**,**g**,**n**), SCG_240 (**c**,**h**,**o**), SCG_220_a (**d**,**i**,**p**) and SCG_240_a (**e**,**l**,**q**).

Table S1 shows the chemical analyses of the different materials. Raw SCG has a percentage of carbon and oxygen equal to 64.9% and 35.1% respectively, and consequently an O/C ratio equal to 0.54. The samples SCG_220 and SCG_240, obtained by hydrothermal treatment, undergo a carbonization process that involves an increase in the percentage of carbon (equal to 83.4 and 86.1%, respectively) compared to the SCG sample, and consequently a decrease in the oxygen content. For the latter, in fact, an O/C ratio equal to 0.2 and 0.16 is found, respectively. The activation treatment determines in SCG_220_a and SCG_240_a samples, in addition to the presence of sodium (equal to 30.25% and 34.3% respectively), a decrease in the carbon content (equal to 32.6 and 25.5% respectively) and

an increase in the oxygen content, which appears to be present in a higher percentage in SCG_240_a sample, with an O/C ratio equal to 1.57, while for SCG_220_a sample this ratio is equal to 1.14. The higher percentage of oxygen (37.2 and 40.2%) indicates a greater presence of OH functional groups which therefore appears to be greater for SCG_240_a sample.

Table S1 also reports the values of the BET surface area for the SCG materials tested, while Figure S1 shows the porosimetric curves determined by mercury intrusion of the SCG and SCG_240_a. Raw SCG have an area of 8.02 m^2/g; moreover, it is predominantly macroporous, with pore sizes in the range 60–150 μm (Figure S1a), while the volumetric contribution of the micropores and mesopores is very low with pore sizes in the range 0.7–4 nm (Figure S2). In contrast, SCG_220 and SCG_240 present lower surface area values equal to 2.89 and 5.14 m^2/g due to the collapse of the microstructure during the hydrothermal treatment. Furthermore, SCG_220 and SCG_240 are micro/mesoporous, with a pore size range between 0.4 and 4 nm and an average porosity value of 2.7 and 1.8 nm, respectively (Figure S2). Similarly, SCG_220_a and SCG_240_a are characterized by a collapse of most of the macropores of size 60–150 μm present in raw SCG and show a pore size of approximately 10 μm (Figure S1b). These materials are characterized by the presence of micro/mesopores with a pore size range between 0.5 and 4 nm (Figure S2) and an average pore radius of 2.31 nm. As shown in Table S1, SCG_220_a and SCG_240_a are characterized by surface area values equal to 10.86 and 5.76 m^2/g, respectively. The increase in surface area compared to non-activated samples is due to the increase in pore volume resulting from the activation treatment with NaOH and subsequent heat treatment at 300 °C, which determines a partial reduction of sodium oxides by carbon with consequent decrease in the C content due to the formation of carbon oxide and sodium carbonate.

3.2. Effect of Hydrothermal Carbonization on the Adsorption Capacity of Spent Coffee Ground

In *Test 1*, raw SCGs and untreated hydrochars produced at 220 and 240 °C were compared in terms of adsorption capacity at an initial MB concentration of 250 mg L^{-1}. As shown in Figure 3, the raw SCG showed a different profile with much higher adsorption capacity compared to the hydrochars ($p < 0.05$). Significantly higher (>2 times) q values were observed for the raw SCG already after 5 min. At the end of the test (3 h), q reached 48.4 (±0.8) mg MB g adsorbent^{-1}, while it was only 15.3 (±1.9) and 8.6 (±3.1) mg MB g adsorbent^{-1} for SCG_220 and SCG_240, respectively. No significant difference was observed in the adsorption behavior of the two hydrochars obtained at different temperatures ($p > 0.05$). For both hydrochars, the highest q values were reached after 20–40 min, while a slight decrease was observed until the end of the test. These results confirm the poor adsorbent properties of untreated hydrochar regardless of production temperature. This behavior is attributable to the collapse of the macroporous microstructure of the raw SCG material and the consequent reduction of the adsorption surface, as shown in Section 3.1. Therefore, activation is required to enhance the adsorption potential of raw hydrochars, e.g., through surface functionalization and/or enhancement of the specific surface area [19]. In contrast, the raw SCG showed good adsorption properties towards MB. The maximum adsorption capacity was about 3 times higher than that reported in a previous study by Franca et al. [20] at an initial MB concentration of 200 mg L^{-1}, which is close to that used in *Test 1*, while the adsorbent concentration was 10 g L^{-1}.

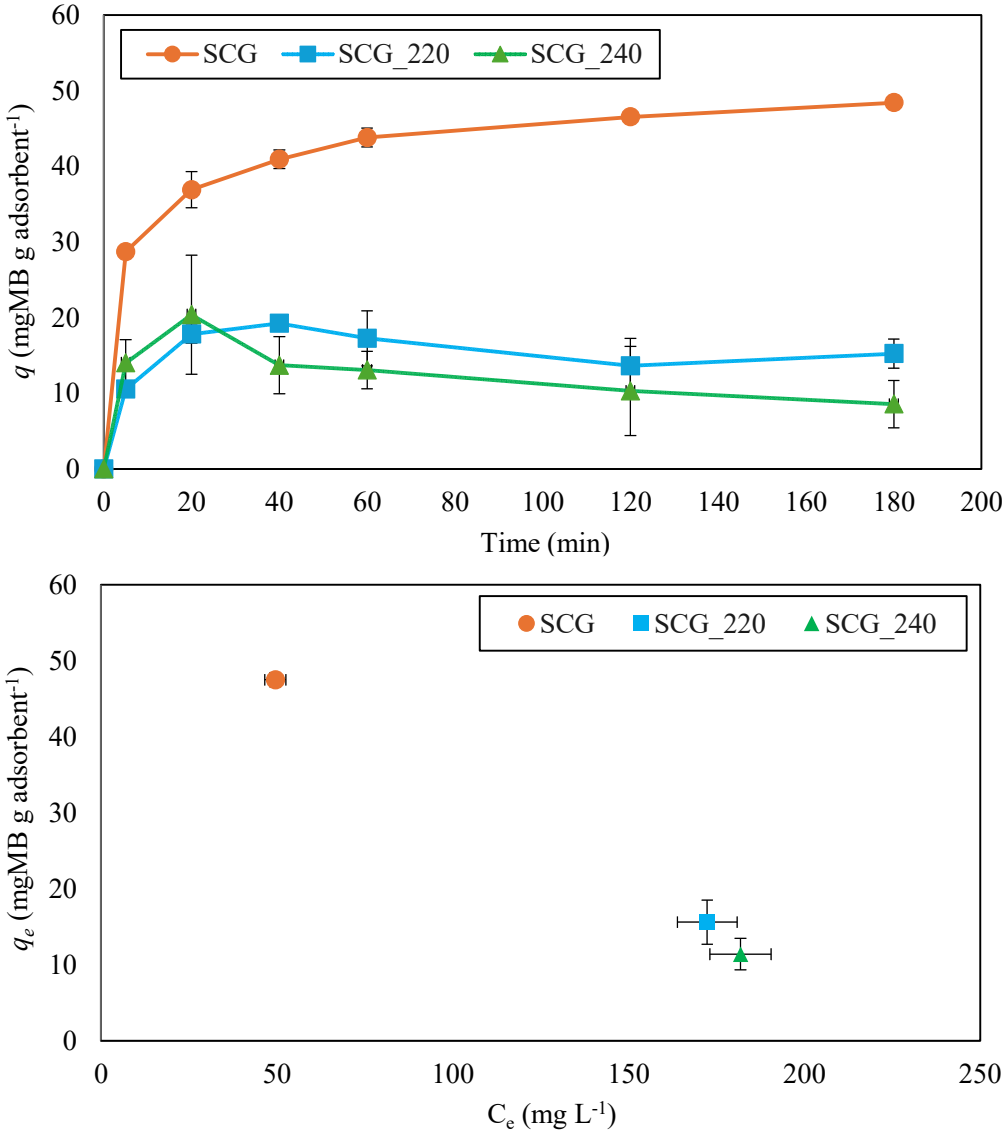

Figure 3. Adsorption capacity profile and equilibrium conditions obtained with raw SCG and related hydrochars obtained at different temperatures.

3.3. Effect of Soft Alkaline Activation on the Adsorption Capacity of SCG Hydrochars

The adsorption capacity of SCG hydrochars was strongly enhanced via soft alkaline activation (*Test 2*). As shown in Figure 4, both activated hydrochars, i.e., SCG_220_a and SCG_240_a, showed high q values already after 5 min (43.5 and 46.5 mg MB g adsorbent^{-1}, respectively), being close to the maximum values reached at the equilibrium (48.3 and 51.5 mg MB g adsorbent^{-1}, respectively). These values were >3 times those reached with untreated hydrochars. Since adsorption occurs mainly on the surface of the adsorbent, the rapid adsorption of MB observed with activated hydrochars is attributable both to the fact that these materials are characterized by a greater surface area than the non-activated ones and to the surface functionalization with hydroxyl groups (higher values of the O/C ratio, Table S1) due to soft alkaline activation. Interestingly, the q_e obtained with activated hydrochars slightly exceeded that obtained with raw SCG, indicating that the SCG hydrochar treated by soft alkaline activation is a better adsorbent than the original waste matrix. However, q_e values for raw SCG and activated hydrochars were close, which is justifiable by the fact that the dimensions of the macropores of the hydrochars have been reduced compared to the original matrix; furthermore, micro-meso pores are present with an average value of the pore radius equal to 2.3 nm, which makes it more difficult for MB

to access. Indeed, MB is a molecule that can be regarded approximately as a rectangular volume of dimensions 1.7 × 0.76 × 0.33 nm = 0.43 nm^3. Although the adsorption capacities of the two activated materials are quite similar ($p > 0.05$), slightly better values were observed with SCG_240_a compared to SCG_220_a at all contact times. This is attributable to the presence of more functional groups (higher O/C ratio) in SCG_240_a, whilst the pore size distribution was similar to SCG_220_a.

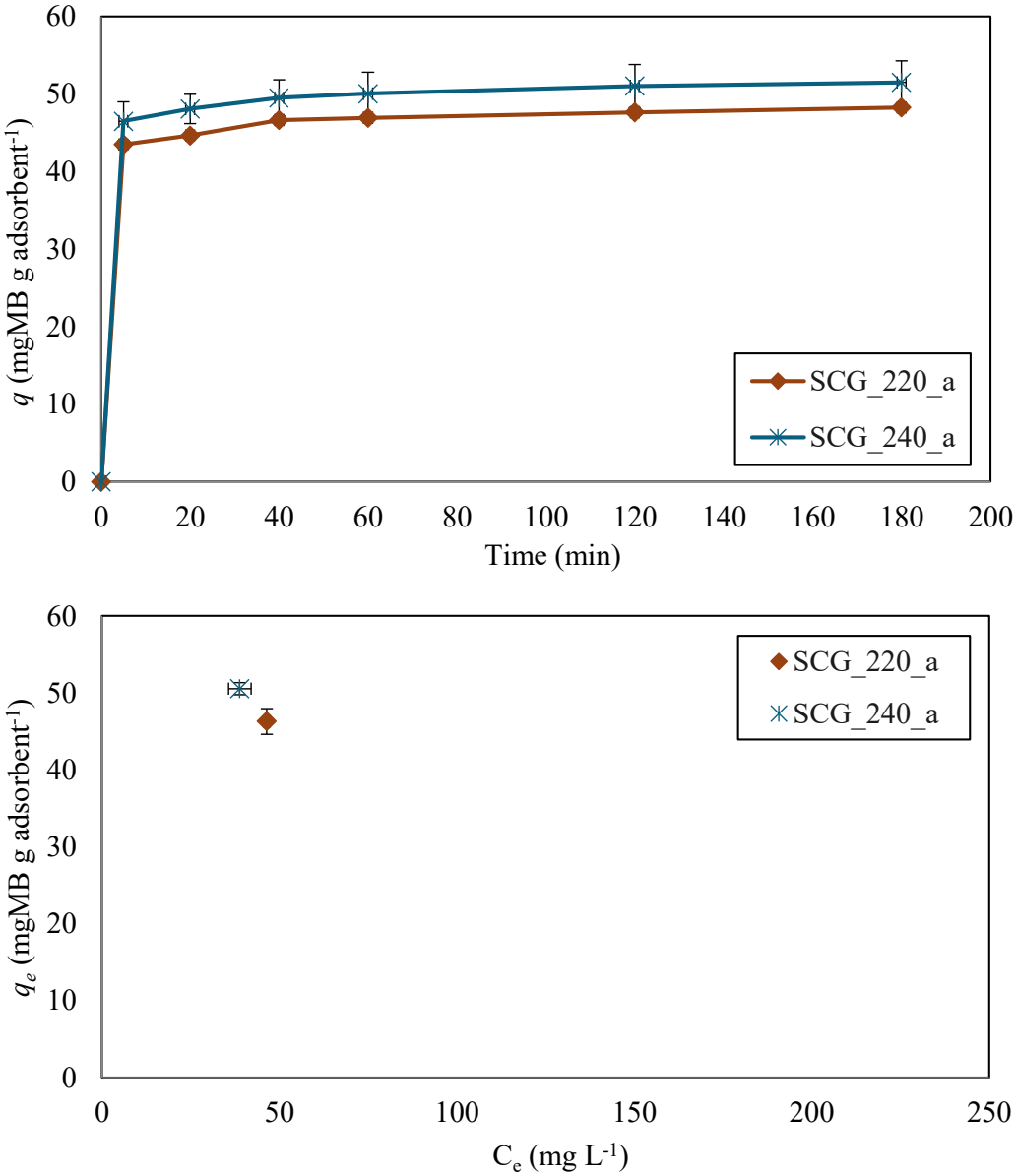

Figure 4. Adsorption capacity of hydrochars from spent coffee grounds obtained at 220 and 240 °C and treated by soft alkaline activation.

Moreover, the higher q_e, activated hydrochars showed higher q values at all contact times compared to the other SCG materials, resulting in faster adsorption. This can be considered advantageous for the treatment of dye-contaminated water, as shorter residence times can be applied to obtain the maximum removal efficiency, resulting in lower treatment volumes.

To better contextualize the performance of the materials produced in this work, a comparison with previously reported adsorption capacities of SCG-derived adsorbents and other low-cost biomass-based sorbents is provided in Table 3. The data indicate that the adsorption capacity achieved after soft alkaline activation compares favourably

with most SCG-based materials reported in the literature and is competitive with several biochars produced from other feedstocks, despite the milder activation conditions applied in this study.

Table 3. Comparison of experimentally measured equilibrium adsorption capacities (q_e) for MB removal from water using SCG-derived and other carbonaceous adsorbents at ambient temperatures.

Material/Feedstock	Treatment/Activation	Experimental Conditions	q_e (mg g^{-1})	Reference
Spent coffee grounds (SCG)	Raw (untreated)	MB 500 mg L^{-1}, 25 °C, pH 5	23.4	[20]
SCG	Soft alkaline activation (NaOH, 300 °C)	MB 250 mg L^{-1}, 20 °C, initial pH 9	~45	[10]
Weed-derived biochar	HNO_3 oxidation	MB 400 mg L^{-1}, 20 °C, pH 7.4	60–65	[21]
Municipal solid waste biochar	Thermal activation	MB 50 mg L^{-1}, 30 °C, pH 6–10	~33	[22]
Lignocellulosic waste biochar	Chemical/physical activation, moderate pyrolysis	MB $\geq$ 200 mg L^{-1}, 20–30 °C, pH 6–9	80–140	[23]
Multilayer graphene-alginate granules	Composite preparation	MB 50 mg L^{-1}, 20 °C, pH 8	183.3	[24]
SCG-derived hydrochar	HTC 240 °C, soft alkaline activation	MB 500 mg L^{-1}, pH 11, 20 °C	97.6	This study

3.4. Effect of pH on Adsorption of Spent Coffee Ground

Although the initial pH of the MB solutions was close to neutrality (6.5–7), the addition of the activated hydrochars increased the pH of the test instantaneously due to the partial release of surface hydroxyl groups and carbonate/bicarbonate species formed during soft alkaline activation, raising the pH of the solution to 11.3 ($\pm$0.1). Therefore, to evaluate whether the different pH had an influence on MB adsorption, batch tests with raw SCG were also performed at pH 11 by adjusting the initial pH of the MB solution (*Test 3*). It was observed that the adsorption spectra of the MB solution at pH 7 and 11 overlapped, indicating no significant impact of the higher pH on spectrophotometric analysis. Similarly, the adsorption capacity profiles of SCG and SCG_240_a obtained at pH 11 were very similar ($p > 0.05$) and reached the same value (~48 mg MB g adsorbent^{-1}) after 3 h (Figure S3). Therefore, no significant difference exists for MB adsorption with SCG between pH 7 and 11.

3.5. Kinetics and Isotherms of Hydrochars from Spent Coffee Grounds

Kinetic tests at 20 °C were performed for the raw SCG and activated hydrochar produced at 240 °C (*Test 4*). The best-fitting kinetic model for both materials was the pseudo-second-order model, with linear regressions showing high R^2 values (0.999–1.000) (Table 4). A complete statistical evaluation (R^2, SSE, RMSE, and χ^2) is reported in Table S2. This behavior indicates chemisorption as the rate-limiting step of the process. In contrast to the pseudo-first-order model, which assumes that the adsorption rate depends on the diffusion of the adsorbate on the adsorbent surface, the pseudo-second order kinetics describes the adsorption of adsorbates onto adsorbents where the chemical bonding (interaction) between adsorbates and functional groups on the surface of adsorbents are responsible for the adsorption capacity of adsorbent [23]. The kinetic parameters k_2 and q_e obtained for the two materials show higher values for SCG_240_a, both being ~3 times higher, describing a much faster adsorption process for the activated hydrochar. Overall, the adsorption of cationic MB on the activated hydrochars was likely governed by multiple contributions: (i) electrostatic attraction promoted by increased surface basicity and carbonate species, (ii) hydrogen bonding involving oxygenated groups introduced after activation, and (iii) π-π interactions between aromatic domains of the carbon matrix and the dye. Given the low BET surface area (Table S1), these chemical interactions are expected to play a dominant role compared to purely surface-area-driven physisorption.

Table 4. Best kinetic and isotherm models for adsorption with the tested SCG adsorbent materials at 20 °C.

Material	Best Model	Linear Equation	R^2	Model Parameters
Kinetics				
SCG	Pseudo-second order	y = −0.0201x + 0.1359	0.999	q_e = 18.2 mg g^{-1} k_2 = 0.0046 min^{-1}
SCG_240_a	Pseudo-second order	y = 0.0193x + 0.0282	1.000	q_e = 51.8 mg g^{-1} k_2 = 0.0132 g mg^{-1} min^{-1}
Isotherms				
SCG_240_a	Langmuir	y = 0.0068x + 0.3589	0.987	K_L = 0.019 L mg^{-1} q_m = 147.1 mg g^{-1} R_L = 0.049

Regarding the isotherm models (*Test 5*), the Langmuir isotherm best described the behavior of SCG_240_a (R^2 = 0.987). This indicates the establishment of a MB monolayer on the surface of the adsorbent with no lateral interaction or transmigration of the adsorbate molecule in the plane of the adsorbent. Based on the model equation, a maximum adsorption capacity of 147.1 mg MB g adsorbent^{-1} can be reached. The positive value of the Langmuir dimensionless constant R_L (Table 4) indicates a favorable adsorption process.

3.6. Impact of Initial Concentration and Temperature on Adsorption with Activated Hydrochar

Increasing the initial concentration of MB from 100 to 750 mg L^{-1} had a positive trend with q_e. By plotting q_e vs. C_e obtained at 20 °C a perfect linear correlation can be observed at initial concentrations between 100 and 500 mg L^{-1}, as shown in Figure 5. In particular, the q_e observed at 500 mg L^{-1} was 97.6 mg MB g adsorbent^{-1}. Under similar experimental conditions (initial MB = 500 mg L^{-1}, 20 °C, alkaline pH), Cuccarese et al. [10] obtained a nearly half q_e for activated raw SCG, which indicates that activated SCG hydrochar performed better than activated raw SCG under alkaline conditions.

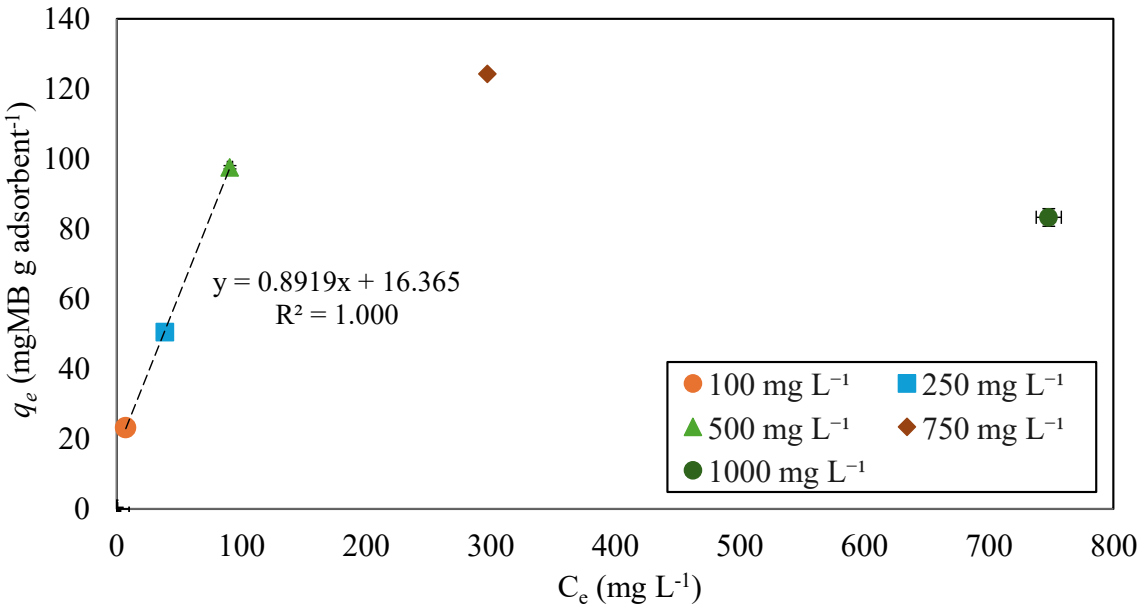

Figure 5. The equilibrium conditions for MB adsorption at 20 °C with activated hydrochar from SCG produced at 240 °C at different initial MB concentrations. The linear regression refers to initial MB concentrations between 100 and 500 mg L^{-1}.

However, the highest q_e of 124.3 mg MB g adsorbent^{-1} was obtained at 750 mg L^{-1}, while a lower value (83.3 mg MB g adsorbent^{-1}) was obtained at 1000 mg L^{-1}. This

decrease at very high dye concentrations is consistent with the well-known behavior of MB, which tends to self-associate into dimers and higher-order aggregates above certain concentration thresholds. Several studies have shown that these aggregated species exhibit lower diffusivity and reduced affinity for adsorption sites compared with monomeric MB, resulting in an apparent decrease in q_e at high initial concentrations [7].

The isotherm test performed with SCG_240_a at different temperatures (Figure 6) showed similar trends up to an initial MB concentration of 500 mg L^{-1}, while for higher concentrations the trend obtained at 40 °C was significantly different from those obtained at lower temperatures. At 40 °C, the value of q_e kept increasing with a linear correlation (R^2 = 0.993) up to the maximum value of 215.6 mg MB g adsorbent^{-1}. Conversely, non-linear trends were observed at 5 and 20 °C. In particular, at a temperature of 5 °C, similar values were observed at 750 and 1000 mg L^{-1}.

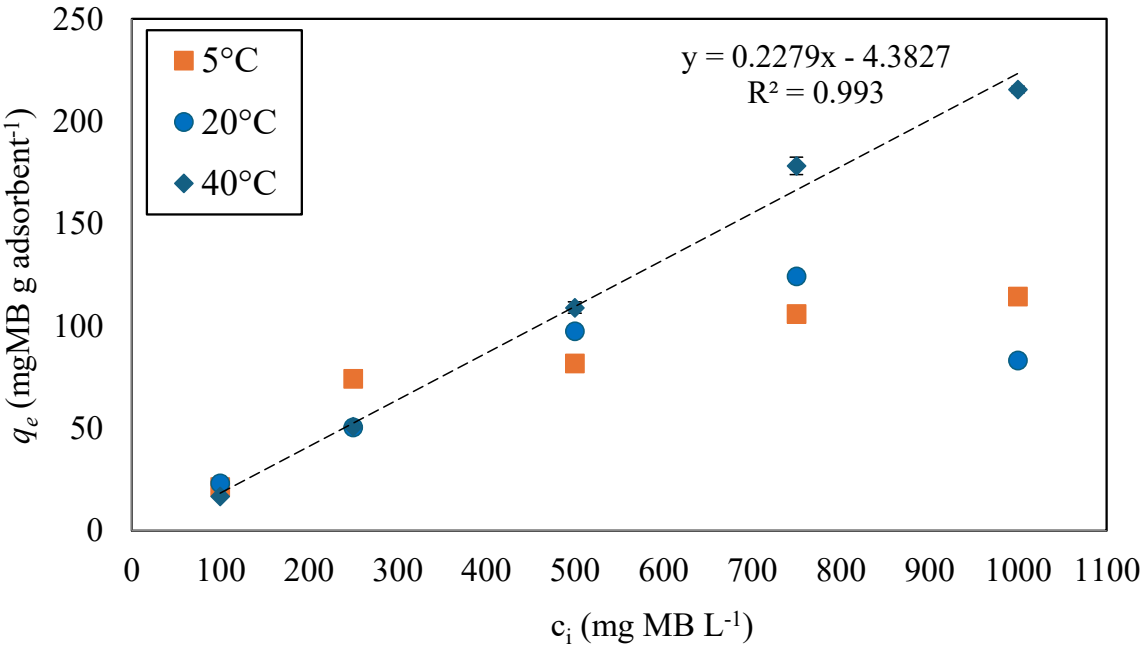

Figure 6. The evolution of the equilibrium adsorption capacity of activated hydrochar from SCG at increasing initial MB concentrations and temperatures. The linear regression refers to experimental values obtained at 40 °C.

Table 5 presents the isotherm models that best fit the experimental data obtained at different temperatures (5–40 °C). Similar to the results obtained at 20 °C, the Langmuir isotherm model was the best fit for MB adsorption at 5 °C (R^2 = 0.991). The Langmuir constant K_L expresses the extent of interaction between the adsorbate and the adsorbent. The higher K_L observed indicates a higher affinity between MB and the activated hydrochar at 20 °C than at 5 °C. This is confirmed by the higher value of q_m obtained at 20 °C, which indicates that a higher amount of MB can form a monolayer on the surface of the adsorbent. Similarly, the data at 5 °C showed a good fit with the Dubinin–Radushkevich isotherm (R^2 = 0.993). The Dubinin–Radushkevich isotherm is based on Polanyi's Potential theory and was developed specifically for microporous solids and gas-solid systems. This model assumes the existence of a force field with a certain potential in the immediate vicinity of the sorbent surface. In these hypotheses, adsorption occurs through a progressive filling of the pore volume, and when the field strength, independently of temperature, is sufficient to compress the solute onto the surface with a partial pressure high enough, condensation can occur [25]. This theory is valid for physical adsorption and non-polar

solutes. Simultaneous fitting to both Langmuir and Dubinin–Radushkevich isotherms was also reported in previous studies on solid-liquid adsorption [26,27].

Table 5. Best-fitting kinetic models at different adsorption temperatures for activated hydrochar from SCG produced at 240 °C.

T (°C)	Best Isotherm Model	R^2	Model Parameters
5	Langmuir	0.991	K_L = 0.017 L mg^{-1} q_m = 120.5 mg g^{-1} R_L = 0.045
	Dubinin–Radushkevich	0.993	β_{DR} = 0.0002 q_s = 112.6 mg g^{-1}
20	Langmuir	0.987	K_L = 0.019 L mg^{-1} q_m = 147.1 mg g^{-1} R_L = 0.049
40	Freundlich	0.941	K_f = 0.058 mg$^{1-1/n}$ L$^{1/n}$ g^{-1} n_f = 0.564

On the other hand, adsorption at 40 °C follows the Freundlich isotherm model (R^2 = 0.941). Conversely to what was observed at lower temperatures, fitting to the Langmuir isotherm was poor (R^2 = 0.569). The Freundlich isotherm typically describes multilayer adsorption on heterogeneous sites. The fitting of the data to the Freundlich isotherm model indicates that temperature increase from 20 to 40 °C had a strong impact on the adsorption mechanism, shifting from monolayer adsorption to the formation of a multilayer with interaction between adsorbed molecules. The Freundlich parameter n_F provides insights on the nature of the adsorption process, which can be linear (n_F = 1), favorable (n_F > 1), unfavorable (n_F < 1), and irreversible (n_F = 0). Based on the n_F value obtained for the Freundlich isotherm at 40 °C (Table 5), the adsorption process was unfavorable. However, an increase in the operating temperature to 40 °C can be recommended when MB concentration in water exceeds 500 mg L^{-1} based on the much higher q_e values obtained compared to lower temperatures (Figure 6).

3.7. Thermodynamics of the Adsorption Process with Activated Hydrochar

The thermodynamics of MB adsorption with activated hydrochar produced at 240 °C (*Test 6*) was investigated through the estimation of several parameters, including the standard enthalpy, entropy, and free energy (Table 6). The linear regression for the calculation of ΔH° and ΔS° had a very good fit with the data points (R^2 = 0.991). The negative values of ΔG° and ΔH° indicate that the process is spontaneous and exothermic. Entropy change ΔS° is also negative, indicating a decreased disorder at the interface between the adsorbent surface and the adsorbed molecules. The negative value of ΔS° suggests physisorption as the main mechanism for MB adsorption onto the activated hydrochar. Physical adsorption onto the adsorbent surface implies a decrease in molecular disorder due to the binding of the adsorbate to active sites through weak intermolecular forces, such as van der Waals interactions, which do not involve significant changes in the electronic orbital configurations of the molecules. This mechanism typically results in a negative entropy change. On the other hand, chemical adsorption may involve the formation of new chemical bonds, which may increase the disorder at the adsorbent surface.

Table 6. Thermodynamic parameters of MB adsorption (250 mg L^{-1}) onto activated SCG-derived hydrochar produced at 240 °C.

T (°C)	ΔG° (kJ mol^{-1})	ΔH° (kJ mol^{-1})	ΔS° (J mol^{-1} K^{-1})
5	−4.347		
20	−4.018	−8.810	−16.151
40	−3.780		

3.8. Practical Remarks

HTC is a promising method for treating organic wastes as they are reduced in volume (>50%) and converted into a carbonaceous solid [28]. Therefore, this technology couples waste minimization and generation of a valuable resource that can be applied for various purposes depending on their characteristics and quality. The conversion of agri-food wastes via HTC therefore appears as a promising strategy to dispose of the residues of agricultural activities and food processing while producing the hydrochar for potential agronomic application and environmental remediation. In this context, the hydrochar produced from SCG and activated via soft alkaline activation which has been tested in this study has shown promising performances. The adsorption capacity observed ranged between 16.8 mg MB g adsorbent^{-1} (MB: 100 mg L^{-1}, 40 °C) and 215.6 mg MB g adsorbent^{-1} (MB: 1000 mg L^{-1}, 40 °C) (Figure 6). These values are even higher than those reported for biochars tested for MB adsorption and produced from weed (q_m < 161.29 mg MB g adsorbent^{-1}) [21] and municipal solid wastes (q_m < 24.4 mg MB g adsorbent^{-1}) [22]. In a previous study, Cuccarese et al. [10] tested a SCG adsorbent treated with soft alkaline activation and observed q_m not exceeding 100 mg MB g adsorbent^{-1} at 250 mg L^{-1} of MB at 20 °C, being nearly twice the q_m obtained in this study with activated SCG hydrochar at the same initial MB concentration (Figure 6). It should be noted that this study does not propose HTC as a method to improve the adsorption capacity of SCG (the opposite occurs, as shown in this study) but rather investigates a potential strategy for reusing the residue of the HTC process (which can be applied for waste reduction). Moreover, it must be considered that the hydrochar generally shows a more condensed structure. HTC generally confers greater stability to the hydrochar, as it promotes the formation of aromatic structures and removes more volatile compounds, making it more resistant to microbial degradation and chemical oxidation compared to its feedstock and less prone to the release of soluble compounds into water [29,30]. This might represent an important advantage of using the activated hydrochar instead of raw SCG over the long term. Additional tests on long-term utilization of raw SCG and hydrochars for adsorption are required to elucidate this aspect. From an application perspective, the implication of soft alkaline activation is not the generation of liquid waste during synthesis, but the increase in pH of the treated water due to the alkaline nature of the activated hydrochar. Therefore, a post-treatment pH adjustment step may be required before discharge or reuse of the treated water. This aspect should be considered in process design and scale-up, particularly for continuous-flow applications. Future work should also assess regeneration and reusability of the activated materials.

4. Conclusions

SCG hydrochar shows potential for environmental remediation applications as an adsorbent for the removal of organic contaminants (e.g., dyes) from water. However, HTC alters SCG functionalities and porous structure, leading to the formation of a condensed microporous solid with a reduced number of functional groups. As a result, the q_e of the SCG hydrochar accounted only for 18–32% of that observed with raw SCG. Soft alkaline activation proved to be effective in enhancing the adsorption performance of SCG hydrochar, as the q_e of the SCG hydrochar reached that of the feedstock. Higher q_e values were ob-

served at increasing the initial MB concentration and temperature. In the investigated range (220–240 °C), HTC temperature had a slight influence on the hydrochar characteristics. The predominant kinetic and isotherm models were the pseudo-second order and Langmuir, respectively, indicating that monolayer adsorption driven by chemisorption was the primary mechanism for MB removal from water with the activated hydrochar. The adsorption capacity was shown to increase with temperature and initial MB concentration (up to 750 mg L^{-1}). Thermodynamics revealed that MB adsorption onto the activated hydrochar is spontaneous and exothermic. Therefore, soft alkaline activation can be considered a sustainable alternative to high-temperature chemical activation for producing adsorbent material from SCG.

Supplementary Materials: The following supporting information can be downloaded at https://www.mdpi.com/article/10.3390/biomass6010006/s1. Table S1—Elemental composition and BET surface area of the SCG adsorbent materials; Table S2—Statistical parameters obtained from data analysis of kinetic and isotherm studies; Figure S1—Porosimetric curves by mercury intrusion of (a) raw SCG and (b) SCG_240_a; Figure S2—BJH pore size distribution obtained by N_2-desorption isotherms; Figure S3—Adsorption capacity profile of raw SCG at initial pH 7 and 11.

Author Contributions: Conceptualization: G.F., F.D.C.; Methodology: All authors; Formal analysis: G.P., G.F., A.D.B., M.C.M.; Investigation: G.P., G.F., F.A., A.D.B., M.C.M., F.D.C.; Resources: G.C., S.M., F.D.C.; Data curation: G.P., G.F., A.D.B., M.C.M., F.D.C.; Writing—original draft preparation: G.P., G.F., F.D.C.; Writing—review and editing: All Authors; Supervision: G.C., D.C., S.M., I.M.M., F.D.C. All authors have read and agreed to the published version of the manuscript.

Funding: Part of this work has been developed within the framework of the project e.INS- Ecosystem of Innovation for Next Generation Sardinia (cod. ECS 00000038) funded by the Italian Ministry for Research and Education (MUR) under the National Recovery and Resilience Plan (NRRP)—MISSION 4 COMPONENT 2, 'From research to business' INVESTMENT 1.5, 'Creation and strengthening of Ecosystems of innovation' and construction of 'Territorial R&D Leaders', CUP F53C22000430001.

Institutional Review Board Statement: Not applicable.

Informed Consent Statement: Not applicable.

Data Availability Statement: Data are available on request from the corresponding author.

Acknowledgments: The authors thank Carla Scarabaggio and Giusy Grasso for their help in the laboratory activities for adsorption tests, and Sebastiana Dal Vecchio and Alberto Colantuono for their help for BET and MIP measurements and SEM-EDX analysis.

Conflicts of Interest: The authors declare no conflicts of interest.

Nomenclature

C_e	concentration of adsorbate at equilibrium (mg L^{-1})
C_{ad}	MB concentration of solute adsorbed at equilibrium (mg L^{-1})
C_0	initial MB concentration (mg L^{-1})
c_i	MB concentration at the beginning of the test (mg L^{-1})
c_f	MB concentration at the end of the test (mg L^{-1})
q	adsorption capacity (mg g^{-1})
q_e	equilibrium adsorption capacity (mg g^{-1})
q_m	maximum adsorption capacity (mg g^{-1})
q_s	theoretical saturation capacity (mg g^{-1})
q_t	adsorption capacity at time t (mg g^{-1})
V	initial volume of the solution for the tests (L)
m	adsorbent weight (g)

k_1	rate constant of pseudo-first order (min^{-1})
k_2	rate constant of pseudo-second order (g mg^{-1} min^{-1})
α	initial adsorption rate constant (mg g^{-1} min^{-1})
β	activation energy constant for chemisorption (g mg^{-1})
k_{fd}	liquid film rate diffusion constant (min^{-1})
k_{dif}	rate constant of intraparticle diffusion (mg g^{-1} $min^{-1/2}$)
K_L	Langmuir equilibrium constant (L mg^{-1})
K_f	Freundlich's constant (mg g^{-1})
K_a	thermodynamic equilibrium constant (dimensionless)
$1/n$	exponent of non-linearity (dimensionless)
b_T	Temkin constant related to the heat of adsorption (J mol^{-1})
E	free energy (kJ mol^{-1})
β_{DR}	Dubinin–Radushkevich constant (mol^2 J^{-2})
M_{MB}	molecular weight of MB (319.89 g mol^{-1})
ΔG°	standard free energy (kJ mol^{-1})
ΔH°	standard enthalpy (kJ mol^{-1})
ΔS°	standard entropy (J mol^{-1} K^{-1})
T	temperature (K)
R	gas constant (8.314 J mol^{-1} K^{-1})
R_L	Langmuir isotherm constant (dimensionless)

References

1. Janissen, B.; Huynh, T. Chemical composition and value-adding applications of coffee industry by-products: A review. *Resour. Conserv. Recycl.* **2018**, *128*, 110–117. [CrossRef]
2. Bermúdez, S.; Voora, V.; Larrea, C. *Global Market Report: Coffee Prices and Sustainability*; International Institute for Sustainable Development (IISD): Winnipeg, MB, Canada, 2022.
3. Acevedo, F.; Rubilar, M.; Scheuermann, E.; Cancino, B.; Uquiche, E.; Garcés, M.; Inostroza, K.; Shene, C. Spent Coffee Grounds as a Renewable Source of Bioactive Compounds. *J. Biobased Mater. Bioenergy* **2013**, *7*, 420–428. [CrossRef]
4. Arias, A.; Ioannidou, S.M.; Giannakis, N.; Feijoo, G.; Moreira, M.T.; Koutinas, A. Review of potential and prospective strategies for the valorization of coffee grounds within the framework of a sustainable and circular bioeconomy. *Ind. Crop. Prod.* **2023**, *205*, 117504. [CrossRef]
5. Bevilacqua, E.; Cruzat, V.; Singh, I.; Rose'Meyer, R.B.; Panchal, S.K.; Brown, L. The Potential of Spent Coffee Grounds in Functional Food Development. *Nutrients* **2023**, *15*, 994. [CrossRef] [PubMed]
6. Yeoh, L.; Ng, K.S. Future Prospects of Spent Coffee Ground Valorisation Using a Biorefinery Approach. *Resour. Conserv. Recycl.* **2022**, *179*, 106123. [CrossRef]
7. Milanković, V.; Tasić, T.; Brković, S.; Potkonjak, N.; Unterweger, C.; Bajuk-Bogdanović, D.; Pašti, I.; Lazarević-Pašti, T. Spent coffee grounds-derived carbon material as an effective adsorbent for removing multiple contaminants from wastewater: A comprehensive kinetic, isotherm, and thermodynamic study. *J. Water Process. Eng.* **2024**, *63*, 105507. [CrossRef]
8. Liang, Y.; Li, H.; Li, X.; Zhang, Q.; Fei, J.; Li, S.; Chen, S. Using recycled coffee grounds for the synthesis of ZIF-8@BC to remove Congo red in water. *Ecotoxicol. Env. Saf.* **2022**, *236*, 113450. [CrossRef]
9. Vo, T.S.; Hossain, M.M.; Kim, K. Natural bamboo powder and coffee ground as low-cost green adsorbents for the removal of rhodamine B and their recycling performance. *Sci. Rep.* **2023**, *13*, 21487. [CrossRef]
10. Cuccarese, M.; Brutti, S.; De Bonis, A.; Teghil, R.; Di Capua, F.; Mancini, I.M.; Masi, S.; Caniani, D. Sustainable Adsorbent Material Prepared by Soft Alkaline Activation of Spent Coffee Grounds: Characterisation and Adsorption Mechanism of Methylene Blue from Aqueous Solutions. *Sustainability* **2023**, *15*, 2454. [CrossRef]
11. Tong, J.; Li, G.; Wang, S.; Li, C.; Wei, J. Functionalized agro-waste for the sustainable remediation of malachite green from wastewater. *Desalination Water Treat.* **2024**, *320*, 100893. [CrossRef]
12. Libra, J.A.; Ro, K.S.; Kammann, C.; Funke, A.; Berge, N.D.; Neubauer, Y.; Titirici, M.M.; Fühner, C.; Bens, O.; Kern, J.; et al. Hydrothermal carbonization of biomass residuals: A comparative review of the chemistry, processes and applications of wet and dry pyrolysis. *Biofuels* **2011**, *2*, 71–106. [CrossRef]
13. Sharma, H.B.; Sarmah, A.K.; Dubey, B. Hydrothermal carbonization of renewable waste biomass for solid biofuel production: A discussion on process mechanism, the influence of process parameters, environmental performance and fuel properties of hydrochar. *Renew. Sustain. Energy Rev.* **2020**, *123*, 109761. [CrossRef]

14. Jalilian, M.; Bissessur, R.; Ahmed, M.; Hsiao, A.; He, Q.S.; Hu, Y. A review: Hydrochar as potential adsorbents for wastewater treatment and CO_2 adsorption. *Sci. Total Environ.* **2024**, *914*, 169823. [CrossRef] [PubMed]
15. Niinipuu, M.; Latham, K.G.; Boily, J.F.; Bergknut, M.; Jansson, S. The impact of hydrothermal carbonization on the surface functionalities of wet waste materials for water treatment applications. *Environ. Sci. Pollut. Res.* **2020**, *27*, 24369–24379. [CrossRef]
16. McKay, G. Adsorption of dyestuffs from aqueous solutions with activated carbon I: Equilibrium and batch contact-time studies. *J. Chem. Technol. Biotechnol.* **1982**, *32*, 759–772. [CrossRef]
17. Liu, Y. Is the Free Energy Change of Adsorption Correctly Calculated? *J. Chem. Eng. Data* **2009**, *54*, 1981–1985. [CrossRef]
18. Ferrari, A.; Robertson, J. Interpretation of Raman spectra of disordered and amorphous carbon. *Phys. Rev. B* **2000**, *61*, 14095. [CrossRef]
19. Khanzada, A.K.; Al-Hazmi, H.E.; Kurniawan, T.A.; Majtacz, J.; Piechota, G.; Kumar, G.; Ezzati, P.; Saeb, M.R.; Rabiee, N.; Karimi-Maleh, H.; et al. Hydrochar as a bio-based adsorbent for heavy metals removal: A review of production processes, adsorption mechanisms, kinetic models, regeneration and reusability. *Sci. Total Environ.* **2024**, *945*, 173972. [CrossRef]
20. Franca, A.S.; Oliveira, L.S.; Ferreira, M.E. Kinetics and equilibrium studies of methylene blue adsorption by spent coffee grounds. *Desalination* **2009**, *249*, 267–272. [CrossRef]
21. Güzel, F.; Sayğılı, H.; Akkaya Sayğılı, G.; Koyuncu, F.; Yılmaz, C. Optimal oxidation with nitric acid of biochar derived from pyrolysis of weeds and its application in removal of hazardous dye methylene blue from aqueous solution. *J. Clean. Prod.* **2017**, *144*, 260–265. [CrossRef]
22. Sumalinog, D.A.G.; Capareda, S.C.; de Luna, M.D.G. Evaluation of the effectiveness and mechanisms of acetaminophen and methylene blue dye adsorption on activated biochar derived from municipal solid wastes. *J. Environ. Manag.* **2018**, *210*, 255–262. [CrossRef]
23. Wang, T.; Jiang, M.; Yu, X.; Niu, N.; Chen, L. Application of lignin adsorbent in wastewater Treatment: A review. *Sep. Purif. Technol.* **2022**, *302*, 122116. [CrossRef]
24. Di Capua, F.; Guglielmucci, D.; Cuccarese, M.; De Bonis, A.; Brutti, S.; Caniani, D.; Mancini, I.M.; Masi, S. Exploring the superior adsorption capacity of multi-layer graphene/alginate granules for the removal of methylene blue dye from water. *Environ. Res.* **2024**, *263*, 119997. [CrossRef] [PubMed]
25. Dubinin, M.M.; Astakhov, V.A. Description of Adsorption Equilibria of Vapors on Zeolites over Wide Ranges of Temperature and Pressure. In *Molecular Sieve Zeolites-II*; American Chemical Society: Washington, DC, USA, 1971; pp. 69–85.
26. Brdar, M.; Šćiban, M.; Takači, A.; Došenović, T. Comparison of two and three parameters adsorption isotherm for Cr(VI) onto Kraft lignin. *Chem. Eng. J.* **2012**, *183*, 108–111. [CrossRef]
27. Chen, X. Modeling of Experimental Adsorption Isotherm Data. *Information* **2015**, *6*, 14–22. [CrossRef]
28. Hämäläinen, A.; Kokko, M.; Tolvanen, H.; Kinnunen, V.; Rintala, J. Towards the implementation of hydrothermal carbonization for nutrients, carbon, and energy recovery in centralized biogas plant treating sewage sludge. *Waste Manag.* **2024**, *173*, 99–108. [CrossRef] [PubMed]
29. Titirici, M.-M.; White, R.J.; Falco, C.; Sevilla, M. Black perspectives for a green future: Hydrothermal carbons for environment protection and energy storage. *Energy Environ. Sci.* **2012**, *5*, 6796–6822. [CrossRef]
30. Luo, X.; Pei, X.; Zhang, X.; Du, H.; Ju, L.; Li, S.; Chen, L.; Zhang, J. Advancing hydrothermal carbonization: Assessing hydrochar's role and challenges in carbon sequestration. *Environ. Res.* **2025**, *270*, 121023. [CrossRef]